Investigation on Mechanically Bi-stable MEMS Devices for Energy Harvesting from Vibrations

Bruno Andò, *Member,* Salvatore Baglio, *SeniorMember,* Gaetano L'Episcopo and Carlo Trigona

***Abstract*—In this paper, mechanically bi-stable MEMS devices are investigated for energy harvesting from mechanical vibrations. This approach is particularly suitable when random, weak, and broadband vibrations in the low frequencies range are considered. These working conditions are in fact quite challenging and are often approached via arrays of linear resonant micro-devices. Our approach allows, with a single device, to efficiently collect kinetic energy in the whole spectrum of frequencies of the incoming signal.**

Bi-stable behaviours are achieved through purely mechanical and fully-compliant micro-mechanisms. Different structures have been analytically and numerically investigated, both in static and dynamic working conditions, and optimized results are proposed.

The advantages of the proposed device, which exploit bi-stable dynamic behaviors, over linear and mono-stable strategies are presented in this paper: in the case of the incoming kinetic energy spread over a large bandwidth and confined at low frequencies, a larger fraction of the input mechanical energy is transferred to the mechanical-to-electrical conversion section of the harvester and, therefore, to the final user.

A complete device design is proposed in this paper by taking into account a dedicated fabrication process which allows to obtain large inertial masses; electrostatic conversion has been considered and embedded into the device to evaluate the device performances in terms of the electric energy scavenged.

***Index Terms*—MEMS, Energy Harvesting, Mechanical Vibrations, Bi-stable Dynamical Systems, Compliant Micro-Mechanisms, Electrostatic Mechanical-to-Electrical Transduction.**

I. Introduction

Ambient energy harvesting has been, in recent years, the recurring target of a number of research efforts aimed to provide an autonomous solution to power up small-scale and low-power electronic devices. Several applications can be listed [1] both in the area of autonomous sensors, such as self-powered sensors [2] or implanted sensor nodes [3], and in general in the field of autonomous micro-systems to recharge the batteries [4], to power up unmanned vehicles [5], to provide energy to human-powered systems [6] and to smart systems [7].

Among different solutions, vibration energy harvesting plays a major role because mechanical vibrations represent one of the most ubiquitously available sources that can potentially deliver a significant amount of energy [8].

Manuscript received December 29, 2011; revised January 19, 2012 and accepted March 12, 2012.

B. Andò, S. Baglio, G. L'Episcopo and C. Trigona are with the D.I.E.E.I. - University of Catania, Viale Andres Doria, 6 - 95125 Catania, Italy.
Email: salvatore.baglio@dieei.unict.it

Color versions of one or more of the figures in this paper are available online at http://ieeexplore.ieee.org.
Digital Object Identifier

Ambient mechanical vibrations come in a large variety of forms such as induced oscillations, seismic noise, vehicle motion, acoustic noise , multi-tone vibrating systems and more generally noisy environments. Sometimes the energy to be collected may be confined in a very specific region of the frequency spectrum, as in the case of rotating machines [9], but very often energy is distributed over a wide spectrum of frequencies. In particular several scenarios exist where a significant fraction of energy is generally distributed in the lower part of the frequency spectrum, below 500 Hz [10].

Vibration generators based on electromagnetic [11], electrostatic [12] and piezoelectric mechanical-to-electric conversion [13] have been suggested in literature [14]. These devices are generally linear resonant devices which show optimal operating conditions when the system is excited at resonance [15]. Thus, the typical approach is based on the design of energy harvesting devices so that the systems linear resonance matches a peak excitation frequency within the source spectrum.

This can induce some inconvenient constraints on both design and fabrication, in particular when micro-systems and low frequencies are addressed [16]. In fact, MEMS resonators can be very sensitive to small dimensional imperfections with resulting disadvantageous fluctuations in efficiency. Moreover, the achievement of very low resonance frequencies (e.g., in the order of few hundred hertz or lower) with a significantly large quality factor is a challenging issue at micro-scale and therefore the devices will generally have a poor efficiency. A further reduction is experienced in the case of wideband vibrations, since linear resonant devices collect energy mainly around their resonance peak [17].

In the attempt to overcome these limits several interesting approaches have been proposed [18]–[20]. One of these adopts multiple linear converters with different frequency responses in order to obtain a wider equivalent bandwidth [19]. Another strategy aims to widen the bandwidth by using a mechanical stopper to nonlinearly limit the amplitude of the resonator [20].

A different approach, proposed in literature in the latter years [21], consists in the exploitation of the properties of non-resonant oscillators characterized by a nonlinear dynamic response. In this specific field, it has been shown that non-resonant mechanical structures, in particular bi-stable systems [22] under proper conditions [23], can provide better performances, compared to linear resonant or generic mono-stable oscillators, in terms of the amount of energy extracted from low frequencies random vibrations with a wide spectrum [24]. Another work presents a piezoelectric micro-machined ultrasonic transducer that can produce power in both linear

and nonlinear working conditions [25]. A bi-stable micro-generator, composed of a MEMS cantilever with a couple of permanent magnets used to induce bi-stable behaviour by exploiting magnetic levitation principle, has been previously proposed by the authors [26].

The solution based on the exploitation of opposing magnetic forces to achieve the nonlinear bi-stable behaviour is particularly suited thanks to the possibility to ”shape” the potential energy function of the system by altering the distance between magnets and therefore to ”tune” its nonlinear behaviour. However, the presence of magnets and, in particular, of ”moving” magnets, is sometimes not desirable whenever the energy harvester is placed close to other electronic devices or magnetic sensors that may be affected by the fluctuations in the magnetic field.

In this work, a novel approach involving purely mechanical, fully-compliant, bi-stable MEMS devices is proposed for vibration energy harvesting.

Nonlinear strategies for energy harvesting with nonlinear micro-structures have been presented in literature [27]–[30]. MEMS devices resembling those considered in this paper have been proposed [31] as bi-stable switches [32]–[34]: all these mechanisms have been actuated by thermal, electrostatic forces or mechanical probes.

Differently from what has been previously proposed in literature, the bi-stable micro-structures proposed in this work are actuated by external random mechanical vibrations, which result in forces acting on an inertial mass placed at the center of the bi-stable micro-mechanism in order to make it ”snap” from one stable equilibrium state to the other one.

The goal of achieving switchings between stable equilibrium states by means of noisy vibrations, thus widening the bandwidth of this device in the frequency-range where vibrations contain more energy [8], will be tackled in this paper to increase the energy conversion efficiency.

Both the MEMS inertial mass displacement and velocity will be taken into account, in fact these quantities are both crucial in the mechanical-to-electrical conversion step: whichever mechanism is used to produce electrical energy, a higher response in terms of displacement and velocity will result in a higher power harvested from random vibrations.

The analytical model of the micro-system will be discussed in section II, where also efforts will be paid to the identification of a suitable micro-fabrication technology that will allow the optimization of the bi-stable behaviour in the subsection II-A. Numerical analyses and their results will be presented in the section III about the static (subsection III-A) and the dynamic (subsection III-B) behaviour of the MEMS device. Afterwards, a realistic case study has been considered taking into account the range of accelerations that can be experienced in automotive applications and a geometrically optimized structure for these applications is proposed and compared with an ”equivalent” mono-stable device in section IV. Finally, the mechanical-to-electrical transduction will be discussed in section V taking into account the electrostatic transduction principle.

II. Device Modeling

The mechanical structure investigated here is composed of a central mass (CM) connected, via two short flexural pivots (LCFP and RCFP), to two slanted rigid links (LRL and RRL). These links are joined, via two short flexural pivots (LSFP and RSFP), to two lateral fixed-fixed beams (LFB and RFB).

The basic structure is shown in fig. 1 where all the acronyms are defined. Flexural pivots allow for the displacements of the entire structure interconnecting, as elastic joints, rigid links (LRL and RRL) and side fixed-fixed beams (RFB and LFB), while the central mass (CM) accounts for the force applied to the structure as a consequence of external accelerations.

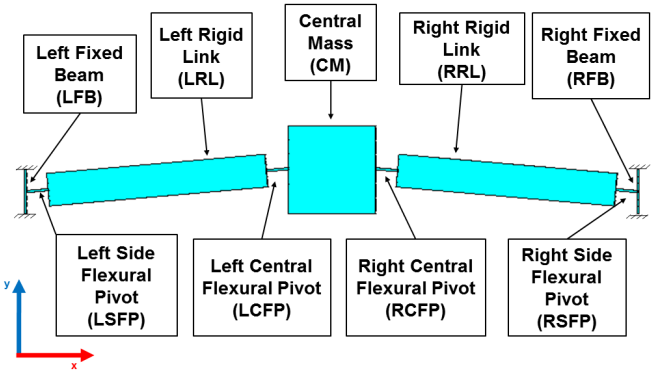

Fig. 1. Two-dimensional structure of the basic device proposed in this work.

Three equilibrium positions can be identified: two stable (’S1’, i.e. the ”fabrication” position, and ’S2’) and one unstable (’U’), as illustrated in fig. 2.

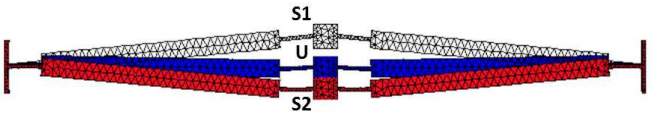

Fig. 2. The initial position (’S1’) is shown together with the unstable (’U’) and the second stable equilibrium position (’S2’) as resulting from FEM simulations.

This section is focused on the analytical model of this device and on the identification of these equilibrium points. The static forces necessary to switch between the two stable states will be derived.

When a force is applied to the central mass along the y-axis, the rigid links LRL and RRL transmit the displacement to the flexural pivots LSFP and RSFP; the displacement along y-axis originated by central mass CM is converted into a motion along x-axis and a rotation thanks to the deformation of the two fixed-fixed beams LFB and RFB.

Because of their elastic deformations, lateral fixed-fixed beams are charged with elastic energy when the system deviates from the initial stable equilibrium state (”S1”); the energy stored is released when the system exceeds the unstable equilibrium position (”U”) and converges to the other stable equilibrium position (”S2”).

By applying the theory of the Pseudo-Rigid Body Model (PRBM) [35] to the previously qualitatively described com-

pliant mechanism, its 1-DOF (Degree of Freedom) model can be derived as in fig. 3.

It should be remarked that only the one dimensional behaviour is studied in this work. Forces along the x-axis are nulled by the device symmetry, while excitations along z, which may eventually induce some precession, are for the moment neglected. These forces will eventually reduce the overall system performance but will not affect the significance of the presented results.

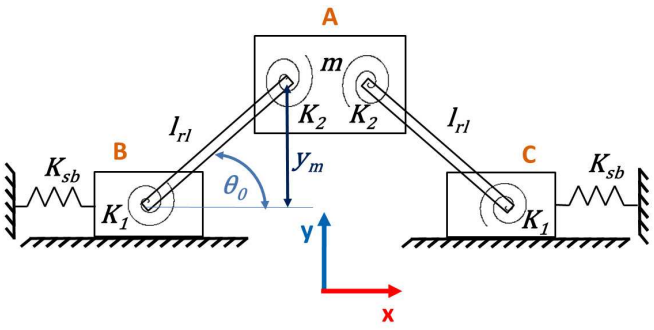

Fig. 3. Pseudo-rigid body model of the micro-structure. The terms K_1 and K_2 refer to the (2), and K_{sb} to the (3).

The general form of the elastic potential energy function can be expressed as:

$$U(y_m) = \frac{1}{2}\Big(2K_1\psi_1^2(y_m) + 2K_2\psi_2^2(y_m) + 2K_{sb}\chi_{sb}^2(y_m)\Big) \tag{1}$$

with:

$$K_i = \frac{(EI)_{l_i}}{l_i} \qquad (i = 1, 2) \tag{2}$$

$$K_{sb} = 192\frac{EI_{sb}}{l_{sb}^3} \tag{3}$$

$$\psi_1(y_m) = \arcsin\left(\frac{y_m}{l_{rl}}\right) - \theta_0 \tag{4}$$

$$\psi_2(y_m) = \arcsin\left(\frac{y_m}{l_{rl}}\right) - \theta_0 \tag{5}$$

$$\chi_{sb}(y_m) = l_{rl}\cos\left(\arcsin\left(\frac{y_m}{l_{rl}}\right)\right) - l_{rl}\cos(\theta_0) \tag{6}$$

where: K_i are the torsional spring constants of small-length flexural pivots (with reference, for the sake of simplicity, only to the left side of the structure it will be: LSFP for $i = 1$ and LCFP for $i = 2$, see fig. 3); K_{sb} is the spring constant of side beams (see fig. 3); E is the Young modulus of Silicon; I_i and I_{sb} are the moments of inertia of flexural pivots and side beams; l_i, l_{sb} and l_{rl} are the length of flexural pivots, side beams and rigid links respectively; y_m is the vertical position of central mass; ψ_1 and ψ_2 are respectively the angular displacements of torsional springs K_1 and K_2 and χ_{sb} is the linear displacement of spring K_{sb}.

By taking into account definitions introduced in (2)-(6), the potential energy function in (1) can be rewritten in a more explicit form as:

$$U(y_m) = (K_1 + K_2)\left[\arcsin\left(\frac{y_m}{l_{rl}}\right) - \theta_0\right]^2 + K_{sb}l_{rl}^2\left[\sqrt{1 - \left(\frac{y_m}{l_{rl}}\right)^2} - \cos(\theta_0)\right]^2 \tag{7}$$

This system has been studied here, both analytically and numerically, in order to assess its bi-stable behaviour and to optimize its performances towards an efficient energy harvesting from environmental vibrations.

An accurate parameter analysis has been performed in order to characterize the effects on the bi-stable behaviour. Among all parameters, a special attention has been payed to the angle θ_0, that is the slope (referenced to the horizontal axis) of the rigid links at the intersection with the side beams. In fact, this angle is one of the fabrication parameters and it strongly affects the bi-stable behaviour as can be seen later in fig. 7.

A. The Potential Energy function and some considerations on the fabrication technology

The goal of this work is focused on obtaining bi-stable behaviour in an inertial micro-system driven by weak forces derived from external vibrations, therefore both a large seismic mass and a highly compliant structure are needed.

A suitable micro-fabrication process must be identified before proceeding further with the numerical investigation; in fact, the final design will have also to adhere to the specific design rules while the micro-system performance will depend on process and materials properties.

The technology considered in this work as a target for future device fabrication is the BESOI (Bulk Etch Silicon On Insulator) process available through the Centro Nacional de Microelectrónica (CNM) of Barcelona (Spain). This is a custom process that makes use of single crystal silicon as primary structural material [36], [37]. This technology promises interesting performance because of the possibility to design a large seismic mass from the whole thickness of the wafer.

The mechanical properties [38] of the structural material (crystal Silicon) used here are reported in tab. I, while fig. 4 illustrates the cross section of this technology.

TABLE I
MECHANICAL MATERIAL PROPERTIES OF SINGLE CRYSTAL SILICON IN BESOI TECHNOLOGY.

Properties	Value
Mass density	2330 kg/m^3
Young's modulus	169 GPa
Poisson's ratio	0.3

An optimization has been carried out over several parameters in order to minimize the acceleration necessary to obtain the switch between the two stable equilibrium configurations and the resulting set of values are reported in table II.

A scheme of the variables listed in table II is shown in fig. 5.

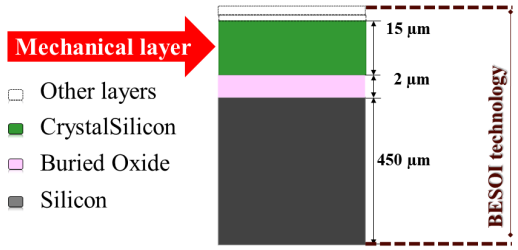

Fig. 4. Cross section of the BESOI technology from Centro Nacional de Microelectrónica (CNM) of Barcelona. Layers not used for the mechanical structure are generically indicated as "other layers". The picture is not in scale.

TABLE II
GEOMETRIC PARAMETERS OF THE MICRO-STRUCTURE IN FIG. 1. THE MICRO-STRUCTURE IS SYMMETRIC ALONG Y-AXIS. A BASIC SCHEMATIC OF THE VARIABLES LISTED IS SHOWN IN FIG. 5.

Variable	Value	Description
θ_0	$5.5°$	Slope of rigid links and flexural pivots
l_{sfp}	$200\ \mu m$	Length of side flexural pivots
l_{rl}	$1500\ \mu m$	Length of rigid links
l_{cfp}	$200\ \mu m$	Length of central flexural pivots
l_{sb}	$150\ \mu m$	Length of side beams
w_{sfp}	$10\ \mu m$	Width of side flexural pivots
w_{rl}	$70\ \mu m$	Width of rigid links
w_{cfp}	$10\ \mu m$	Width of central flexural pivots
w_{sb}	$10\ \mu m$	Width of side beams
t	$15\ \mu m$	Thickness (except the central mass)
t_{cm}	$467\ \mu m$	Thickness of the central mass

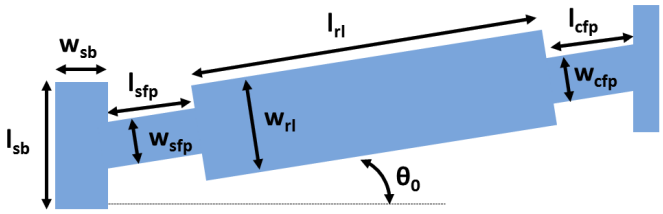

Fig. 5. Basic schematic of the variables listed in the tab. II for the micro-structure in fig. 1. The picture is not in scale.

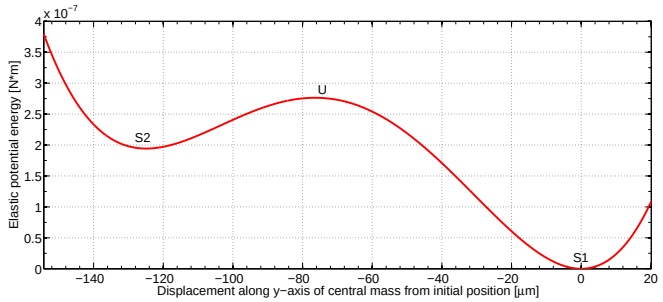

Fig. 6. Elastic potential energy evaluated by PRBM with $\theta_0 = 5.5°$. The stables (S1 and S2) and the unstable (U) equilibrium positions are marked.

The potential energy function is shown in fig. 6.

The bi-stable potential is not symmetrical, this is due to the slope θ_0 assigned as a design parameter to the junction between the flexures and the rigid links. This means that flexural pivots are deflected in the second stable equilibrium position "S2" and, consequently, the torsional springs K_1 and K_2 are not at rest and give a nonzero contribution to the elastic potential energy. As a consequence, a higher energy threshold must be overcome to switch from S1 to S2 than from S2 to S1.

The asymmetrical trend in fig. 6 can be seen as the sum of two contributions: one, symmetrical, due to the spring K_{sb} and another, asymmetrical, generated by torsional springs K_1 and K_2.

The result of parametric analysis is reported in fig. 7 where the influence of the parameter θ_0 on the bi-stable behaviour of the device is shown.

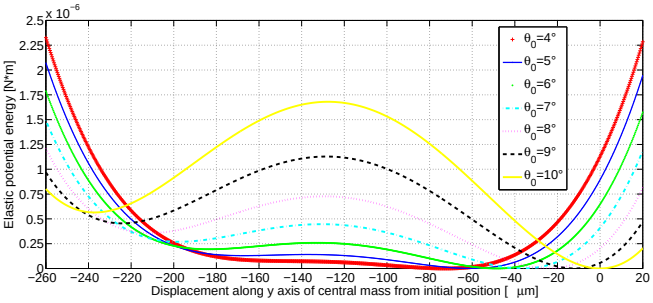

Fig. 7. Elastic potential energy evaluated for different values of the parameter θ_0. For $\theta_0 = 4°$ and the other parameters in table II, the micro-structure has a mono-stable behaviour. Results refer to parameters different from those in the tab. II.

III. NUMERICAL ANALYSIS AND RESULTS

Finite Elements Model (FEM) analyses have been carried out in order to investigate bi-stable behaviour and to confirm results obtained from PRBM.

A. Static modeling

The methodology adopted in these simulations consists of nonlinear static mechanical analyses: a very small displacement along y-axis is applied, step by step, to the central mass of the micro-structure and the resultant reaction force along y-axis on central mass is computed. The positions where reaction force is equal to zero are the equilibrium points according to equation (8).

$$F_y = \frac{dU(y)}{dy} \tag{8}$$

where F_y is the reaction force along y-axis and $U(y)$ is the elastic potential energy. From (8), elastic potential energy is obtained by numerical integration of reaction forces over displacements along y-axis.

Figure 8 shows reaction force along y-axis on central mass when its position changes, while fig. 9 presents results of numerical integration of reaction forces.

Figure 9 confirms the expected bi-stable behaviour. A small difference between the equilibrium positions evaluated from PRBM and from FEM is observed, this is due to the over-estimation of the energy contribution of flexural joints in the PRBM [35].

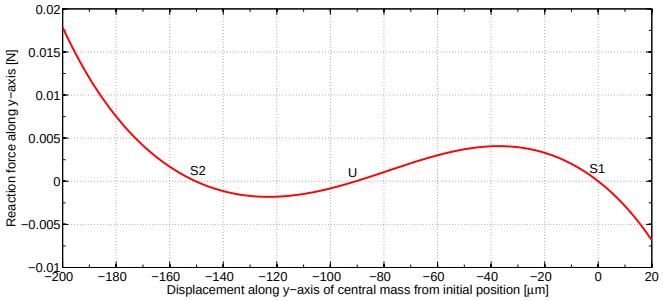

Fig. 8. Reaction force on central mass after displacement numerically evaluated by FEM.

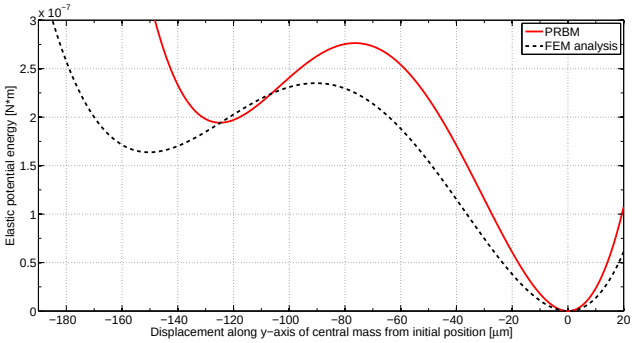

Fig. 9. Elastic potential energy numerically evaluated by FEM (dashed line) compared with the potential (continuous line) obtained from PRBM (fig. 6).

The deformed structures in U and in S2 are shown in figure 2 together with the undeformed system in S1. Table III summarizes the results computed by PRBM and FEM analyses for the equilibrium configurations and the critical static forces necessary to switch between the two stable equilibrium positions.

TABLE III
SUMMARY OF PRBM AND FEM RESULTS ABOUT EQUILIBRIUM POSITIONS AND CRITICAL FORCES.

	PRBM	**FEM**
1st stable equilibrium	$0\ \mu m$	$0\ \mu m$
Unstable equilibrium	$-76\ \mu m$	$-90\ \mu m$
2st stable equilibrium	$-125\ \mu m$	$-150\ \mu m$
Critical force (1st to 2nd)	$5.7\ mN$	$4.07\ mN$
Critical force (2nd to 1st)	$2.6\ mN$	$1.81\ mN$

B. Dynamic modeling

In order to investigate dynamic behaviours of the bi-stable micro-structure in the case of random input vibrations, the corresponding stochastic differential equations (SDEs) model has been considered.

The nonlinear dynamic model is indicated in (9).

$$m\ddot{y} + c\dot{y} + \Psi(y) = -ma_{ext} \tag{9}$$

where m is the central mass of the system, c is the damping coefficient, y is the displacement of central mass along y-axis respect to the external frame, a_{ext} is the input acceleration applied to the external frame and $\Psi(y)$ is the nonlinear elastic term expressed by (10):

$$\Psi(y) = \frac{dU(y)}{dy} \tag{10}$$

where $U(y)$ is the elastic potential energy function, evaluated via a fourth-order polynomial fitting of the FEM results shown in fig. 9.

From (9), the two-dimensional stochastic differential equations system in Itō form [39] can be derived (11):

$$\begin{cases} dy = y_v dt \\ dy_v = \frac{1}{m}\Big[- cy_v - \Psi(y)\Big]dt + \frac{\sigma}{m} dW_t \end{cases} \tag{11}$$

where y_v represents the velocity of the central mass, W_t represents the Wiener process, which increments by dW_t. Wiener process models the stochastic input due to external mechanical random vibrations. Finally σ represents the diffusion coefficient which set the magnitude of the stochastic input a_{ext} by (12) [40]. The input signal is therefore modeled as:

$$a_{ext} = \frac{\sigma}{m}\frac{dW_t}{dt} = \frac{\sigma}{m}\epsilon_t \frac{1}{\sqrt{dt}} \tag{12}$$

where ϵ_t is a dimensionless, random, serially uncorrelated, normally distributed variable.

The Euler-Maruyama method has been used to solve numerically SDEs model in (11) by using Matlab and to evaluate the dynamic behaviour of the system [39]. Setting $\sigma = 12\ \mu N\sqrt{s}$, the integration time step $t_s = 1\ \mu s$ and taking into account BESOI technology parameters, the results shown in fig. 10 have been obtained.

Bi-stable behaviour is evident in the simulated dynamics.

In order to compare the behaviour of the device proposed with an equivalent mono-stable system, simulations benchmarks have been performed by considering the same structure as in Tab. II but having $\theta_0 = 0°$. This device is regarded as "equivalent" because it is of the same geometrical parameters of the proposed bi-stable structure with the exception of the base angle θ_0 which is equal to zero in order to induce a mono-stable elastic behaviour. In fact it is shown in fig. 7 that for $\theta_0 = 0°$ the potential function is mono-stable, in these conditions the behaviours are similar (apart some obvious distortions) to those of a conventional linear resonant oscillator.

The same random stochastic input signal has been applied to both systems. Power Spectral Densities (PSDs) of the mass displacement are shown in fig. 11 for both the bi-stable and the mono-stable system.

It can be observed that bi-stable system exhibits both a wider spectrum and a higher gain, at low frequencies, than the mono-stable one which shows the peak similarly to a linear resonant device.

Therefore, when subjected to vibrations with wide spectrum at low frequencies, the bi-stable device is capable to scavenge a larger fraction of the incoming energy than the equivalent mono-stable device.

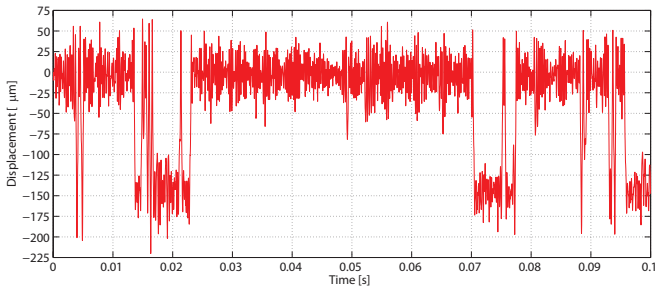

(a)

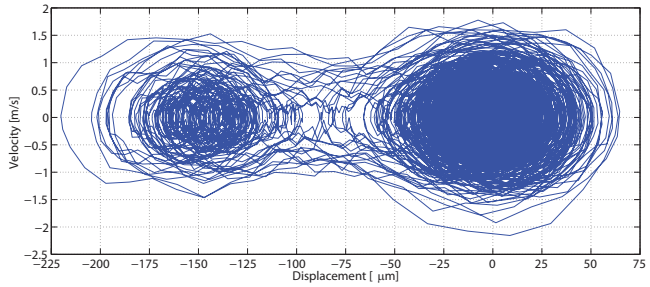

(b)

Fig. 10. Results from numerical evaluation of SDEs model by Euler-Maruyama method. Time series of the displacements (a) and trajectory map of the two system states variables (displacement and velocity) under stochastic input dW_t (b). The bi-stable behaviour is clearly visible.

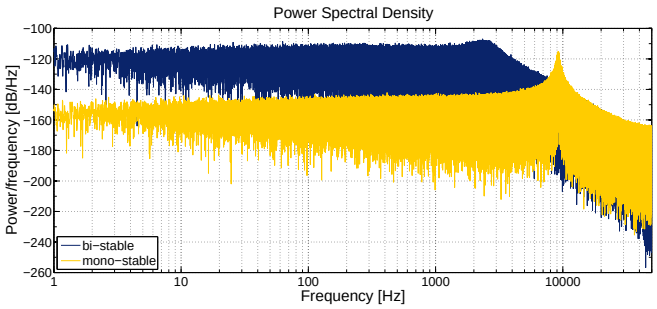

Fig. 11. Comparison between power spectrum densities of central mass displacements of bi-stable micro-structure and mono-stable one under the same stochastic stimulus dW_t.

This difference will result also in a large amount of electrical energy whatever mechanical-to-electrical energy conversion strategy will be used in this energy harvester.

IV. Design of vibration MEMS energy harvesting

In this section, the design of a bi-stable MEMS structure that can profitably harvest energy from low level vibrations, whose energy is spread over a large bandwidth at low frequencies, is proposed.

Several scenarios are considered, including automotive, where vibrations appear as a noisy signal [8] with acceleration peak of about 12 m/s^2 and bandwidth of few hundreds Hertz, eventually up to about 500 Hz.

The design goal is focused on a bi-stable MEMS device that can show low critical forces, mechanical robustness, rejection of unwanted vibrational modes and a limited occupation of wafer area taking into account the BESOI technology parameters.

The worst case to allow switching between stable states is represented by the critical force required to statically commutate from S1 to S2 and that can be evaluated by FEM (see for example tab. III in the case of the previous structure), while a more accurate estimation of the minimal forces required to obtain switching must be performed by taking into account the dynamic behaviour.

The design strategy will be based on FEM simulations results to estimate the force level to be applied to the inertial mass in order to induce switching between the two stable equilibrium states of the device; the worst case, represented by the commutation from S1 to S2, will be obviously taken into account. The dynamic behaviours will therefore be taken into account to refer these results to the external acceleration a_{ext}.

The basic bi-stable structure studied in the previous section has been considered as first device candidate. For this device it has been not possible to satisfy all the design goals as the minimum acceleration level required for inducing switching was larger than the considered design goal.

A modified structure has been therefore considered where a different geometry for the flexural beam has been taken into account in order to increase the device flexibility. The fixed-fixed beams (LFB and RFB) have been replaced by a rigid part (Left Rigid Part, LRP, and Right Rigid Part, RRP) interconnecting respectively each of the original side flexural pivots (LSFP and RSFP) to two flexural pivots (Left Side Upper Flexural Pivot, LSUFP, and Left Side Lower Flexural Pivot, LSLFP, Right Side Upper Flexural Pivot, RSUFP, and Right Side Lower Flexural Pivot, RSLFP). These two additional flexural pivots are joined to two fixed-fixed beams (Left Upper Fixed Beam, LUFB, Left Lower Fixed Beam, LLFB, Right Upper Fixed Beam, RUFB, and Right Lower Fixed Beam, RLFB). Figure 12 illustrates the aforesaid changes on the micro-structure and the nomenclature of the new components of the micro-structure, for the left side.

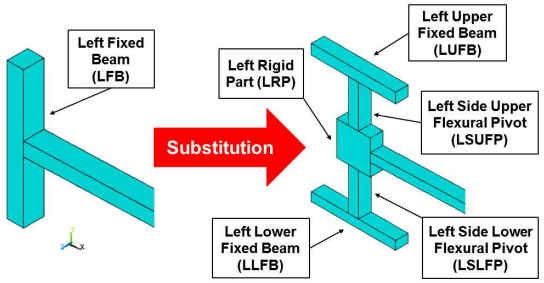

Fig. 12. Basic illustration of the substitutions, only for the left side, made to the micro-structure in fig. 1 in order to make it more flexible. Changes and nomenclature are analogous on the right side.

In order to improve the mechanical stability of the micro-structure and to reduce the incidence of some unwanted vibrational modes, the number of arms that hold the central mass has been increased to four and the total thickness of the BESOI wafer (467 μm) has been exploited in the implementation of

these arms. This also allows the use of larger central masses without affecting the robustness of the structure and its main vibrational mode (along y-axis). A complete picture of the new micro-structure is shown in fig. 13.

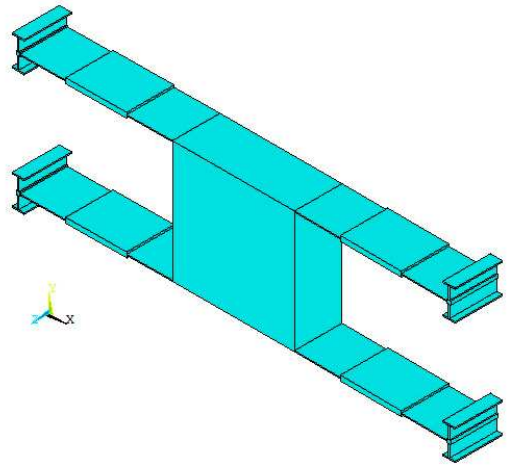

Fig. 13. Three-dimensional model of the new proposed micro-structure.

Thanks to these substitutions, the new structure is more compliant than the previous one and its increased mechanical flexibility leads to lower values of critical forces required for commutations between stable states.

A parameter analysis like the one shown in fig. 7 gives the optimum parameters in tab. IV for the structure shown in fig. 13. A basic schematic of the variables listed in tab. IV is illustrated in fig. 14. Switchings between the two stable states is now allowed by external vibrations with peak acceleration of 12 m/s^2. The square central mass of 1200 μm side length allows to convert the external acceleration into a force applied to the structure. The micro-structure occupies an area 3.74 mm long and 1.33 mm wide.

TABLE IV
GEOMETRIC PARAMETERS OF THE MICRO-STRUCTURE IN FIG. 13. THE MICRO-STRUCTURE IS SYMMETRIC ALONG Y-AXIS. A BASIC SCHEMATIC OF THE VARIABLES LISTED IS SHOWN IN FIG. 14.

Variable	Value	Description
θ_0	0.5°	Slope of rigid links and flexural pivots
l_{sfp}	450 μm	Length of side flexural pivots
l_{rl}	600 μm	Length of rigid links
l_{cfp}	450 μm	Length of central flexural pivots
l_{rp}	35 μm	Length of rigid parts
l_{sufp}	120 μm	Length of side upper flexural pivots
l_{slfp}	120 μm	Length of side lower flexural pivots
l_{ufb}	120 μm	Length of upper fixed beams
l_{lfb}	120 μm	Length of lower fixed beams
w_{sfp}	10 μm	Width of side flexural pivots
w_{rl}	60 μm	Width of rigid links
w_{cfp}	10 μm	Width of central flexural pivots
w_{rp}	35 μm	Width of rigid parts
w_{sufp}	12 μm	Width of side upper flexural pivots
w_{slfp}	12 μm	Width of side lower flexural pivots
w_{ufb}	12 μm	Width of upper fixed beams
w_{lfb}	12 μm	Width of lower fixed beams
t	467 μm	Thickness of the entire structure

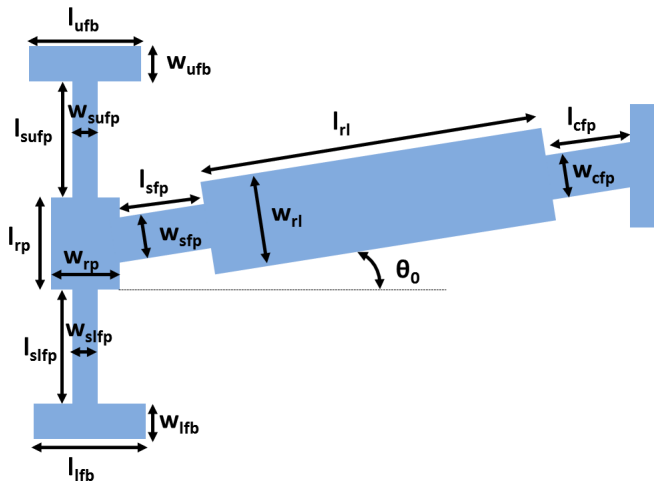

Fig. 14. Basic schematic of the variables listed in the tab. IV for the micro-structure in fig. 13. The picture is not in scale.

Results of the reaction forces against structure displacements, evaluated by FEM analysis, and the corresponding elastic potential energy are shown in fig. 15.

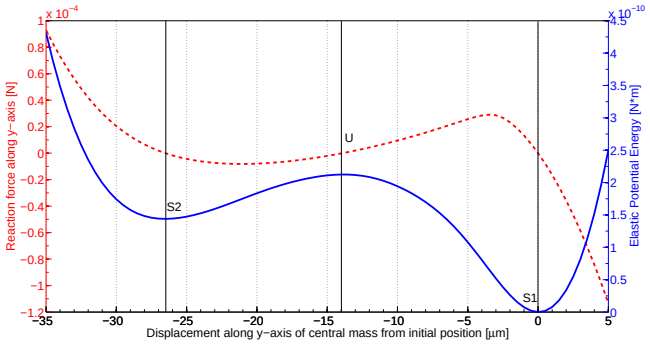

Fig. 15. Reaction force (dashed line) on central mass and elastic potential energy (continuous line) evaluated by FEA for configuration on table IV of the micro-structure proposed in figure 13. Equilibrium positions are indicated.

The unstable equilibrium position U is at -13.75 μm from initial position along y-axis and the second stable equilibrium position S2 is at -26.7 μm from initial position. The critical force to switch from S1 to S2 is 29.1 μN, while the required static force to commutate from S2 to S1 is about 8.2 μN.

Several dynamic analyses, using the model in (11), have been performed in order to characterize the behaviours of the new structure in fig. 13, when the parameter values reported in tab IV are adopted.

The number of commutations between the two stable equilibrium states as a function of the RMS value of the external acceleration, considered as a stochastic signal, has been considered as quantifier of the device performance. In fig. 16 the results obtained are shown in terms of average number of switching events, over a simulation time of 60 s, and standard deviation. The largest energy value reported in the horizontal axis corresponds to peak accelerations up to about 14 m/s^2.

A comparison between this bi-stable behaviour and its

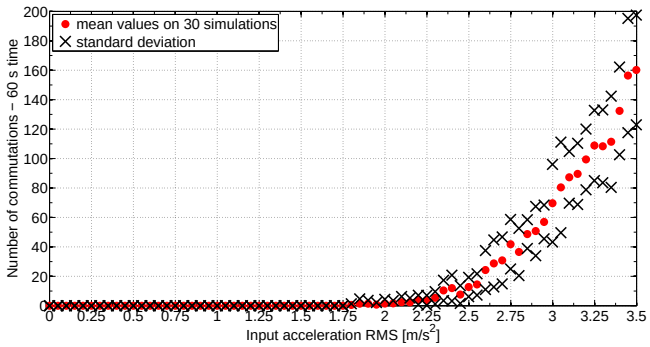

Fig. 16. Results from several stochastic analyses for accelerations having different RMS values. Points represent the mean values of the number of commutations between stable equilibrium states in a time interval of 60 s and 30 simulations for every simulated value of input peak accelerations; while "x" represent the standard deviation.

"equivalent" mono-stable is performed again by taking into account the same structure but having $\theta_0 = 0°$. The elastic potential of the equivalent mono-stable device is shown in fig. 17 in comparison with the elastic potential of the bi-stable micro-structure.

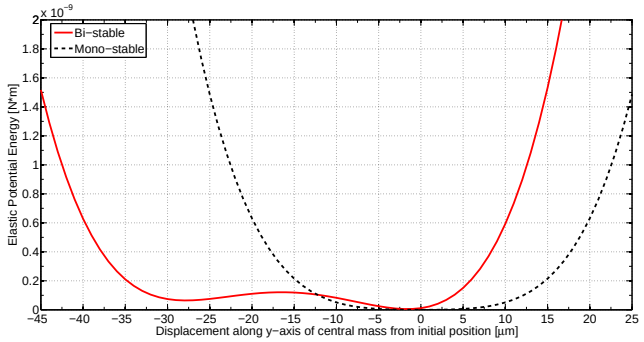

Fig. 17. Elastic potential energy numerically evaluated by FEM of the mono-stable device (dashed line) compared with the potential (continuous line) of the bi-stable one.

In fig. 18 the PSDs of central mass displacements are reported both for the bi-stable and for the mono-stable device: the case of a stochastic input acceleration smaller than the minimum value allowing for device switching is shown in fig. 18a; the case of input acceleration large enough to allow commutations between the two stable states of the device are shown in fig. 18b.

The integral of the PSD of central mass displacement in the frequency range of interest ($0.1\ Hz$–$500\ Hz$) represents the mechanical energy scavenged by the micro-structure from the random environmental vibrations; the device performance is estimated as the ratio between the energy transferred to the mechanical-to-electrical conversion system and the external vibrations energy in the frequency range of interest.

A slightly better performance at low frequencies is observed in the mono-stable structure when the bi-stable one does not switch between its stable equilibrium states (fig. 18a): this is due to a lower resonant frequency with respect the bi-stable one. When the bi-stable structure begins to switch between its

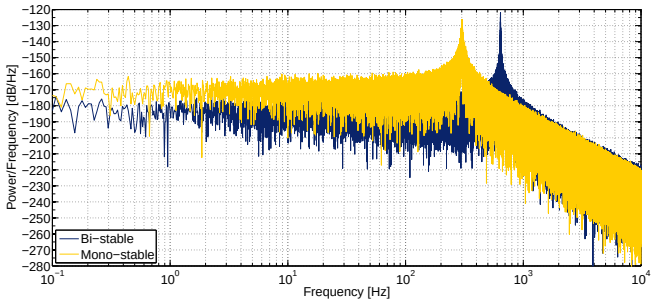

(a) Simulation results: plot of PSD of central mass displacement for the bi-stable (blue curve) and the mono-stable (yellow curve) in the case of under-threshold excitation (acceleration peak value of about $4\ m/s^2$) when the bi-stable system oscillates around its first stable equilibrium state.

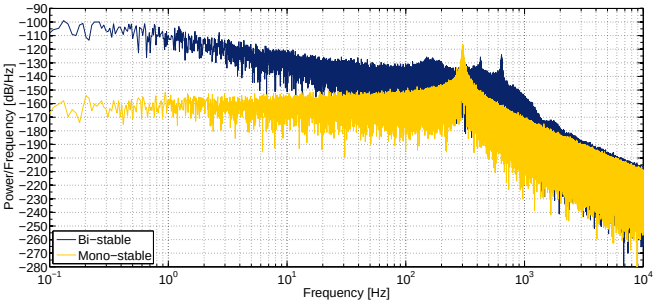

(b) Simulation results: plot of PSD of central mass displacement for the bi-stable (blue curve) and the mono-stable (yellow curve) in the case of above-threshold excitation (acceleration peak value of about $12\ m/s^2$) when the bi-stable system bounces between its two stable states.

Fig. 18. Simulation results of the comparison between the optimized bi-stable device and the same structure operating in the mono-stable mode ($\theta_0 = 0°$) with respect to a stochastic vibration applied to the system in the case of under-threshold excitation (a) and above-threshold excitation (b).

stable equilibrium states, its behaviour is considerably more efficient than the mono-stable one (fig. 18b).

In fig. 19 the total energy gathered is plotted, for both the mono-stable and the bi-stable structures, as a function of the RMS value of input acceleration. The energy is evaluated as the normalized PSD integral, in the frequency range of $0.1\ Hz$–$500\ Hz$ of the central mass displacement. Normalization is performed with respect to the input acceleration energy in the same frequency range.

In fig. 19 it is shown that the bi-stable device harvests more mechanical energy than the mono-stable one as soon as the excitation signal becomes large enough to induce switchings between the two stable equilibrium states.

V. Considerations on Mechanical-to-Electrical Energy Conversion

The electrostatic mechanical-to-electrical transduction strategy is considered for this device. Voltage constrained [41], in-plane overlap varying [14] interdigitated capacitors have been designed on both the upper and lower sides of the central mass in order to exploit the displacements along y-axis in the energy transduction. A three dimensional model of the device is illustrated in fig. 20.

The fingers of the capacitors have a total thickness of $467\ \mu m$, as all the three layers of the BESOI wafer (see fig. 4)

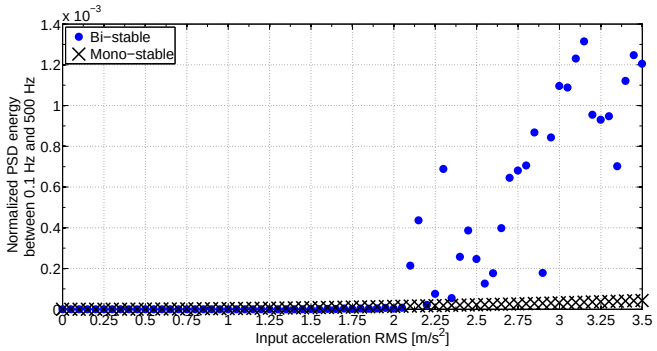

Fig. 19. Energy of central mass displacements normalized with input energy from vibrations versus the RMS value of the input acceleration signal. Points represent the computed values for the bi-stable micro-structure at each acceleration peak value, while the "x" for the mono-stable device.

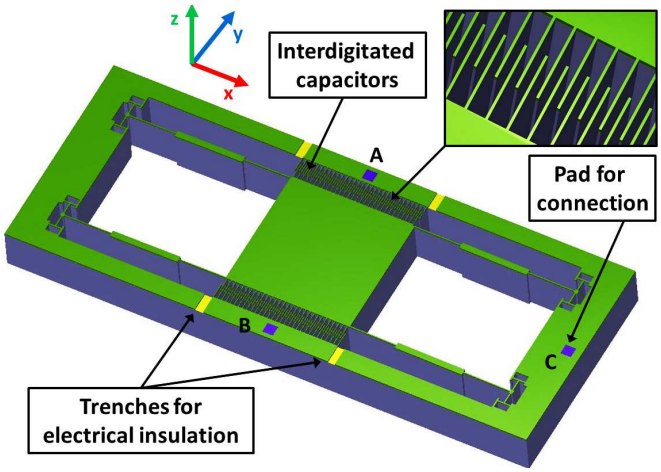

Fig. 20. Three dimensional model of the device incorporating the micro-structure in fig. 13 and the mechanical-to-electrical transduction mechanism. The letters "A", "B" and "C" indicate the pads for the electrical connection of the plates of the interdigitated capacitors.

have been considered. This gives higher mechanical robustness to the fingers and increases the inertial mass applied to the micro-structure. However, only $15\ \mu m$ in single crystalline silicon are exploited for the electrical capacitors because of electrical insulation due to buried oxide layer between the single crystalline silicon and the substrate.

The two overlap varying interdigitated capacitors C_{AC} (between the stator "A" and the rotor "C" in fig. 20) and C_{BC} (between the stator "B" the rotor "C" in fig. 20) are defined in (13) and in (14) [42]:

$$C_{AC}(y) = 2\frac{N_f \epsilon_0 t_f \big(l_{f0} - y\big)}{g} \tag{13}$$

$$C_{BC}(y) = 2\frac{N_f \epsilon_0 t_f \big(l_{f0} + y\big)}{g} \tag{14}$$

where N_f is the number of fingers (on the rotor side of the capacitor), ϵ_0 is the electrical permittivity of air, t_f is the thickness of the electrical layer in the capacitor, g is the air gap, l_{f0} is the length of the overlap between two fingers facing each other and y is the displacement of the central mass along the y-axis from its initial position.

Taking into account the applied mechanical-to-electrical conversion system, the model in (9) modifies [8] in (15) :

$$m\ddot{y} + c^*\dot{y} + b_e(y) + \Psi(y) = -ma_{ext} \tag{15}$$

The parameter c^* in (15) represents the mechanical damping caused predominantly by the slide film effect in the interdigitated capacitors and is stated by the (16) [43].

$$c^* = 4\frac{N_f \eta t_f l_{f0}}{g} \tag{16}$$

where η is the dynamic viscosity of air ($\eta = 18\ \mu Pa \cdot s$).

The term b_e is the electrical damping that models the effect of the electrical polarization of the two interdigitated capacitors $C_{AC}(y)$ and $C_{BC}(y)$ on the mass movement and is defined by (17) [8]:

$$b_e(y) = \frac{\epsilon_0 N_f t_f}{g} {V_{AC}}^2 - \frac{\epsilon_0 N_f t_f}{g} {V_{BC}}^2 \tag{17}$$

where the terms V_{AC} and V_{BC} are respectively the polarization voltages of the capacitors C_{AC} and C_{BC}. The signs in (17) indicate the directions of the damping forces from the two capacitors (when each of them is polarized) that are opposite to the direction of the motion of the central mass. According to the (13)–(14) and considering the bi-stable dynamic operation of the proposed device, if any overshoots in the displacement of the central mass are neglected, the capacitance C_{AC} presents its maximum value in S1 while C_{BC} its minimum; analogously, in S2, C_{AC} is at its minimum while C_{BC} at its maximum.

On the basis of the operating cycle of voltage constrained electrostatic mechanical-to-electrical transduction systems [44], the voltage V_{AC} is equal to the applied voltage V_{in} only when the central mass goes from S1 to S2 and in the other cases V_{AC} is equal to $0\ V$, while V_{BC} is equal to V_{in} when the central mass comes from S2 to S1 and in the other cases V_{BC} is equal to $0\ V$. The energy harvested respectively by the capacitor C_{AC} in each cycle of commutation from S1 to S2 and by the capacitor C_{BC} in each cycle of commutation from S2 to S1 are expressed by E_{AC} and E_{BC} in (18) and (19) [41]:

$$E_{AC} = \frac{1}{2}\big(C_{AC}(S1) - C_{AC}(S2)\big){V_{in}}^2 \tag{18}$$

$$E_{BC} = \frac{1}{2}\big(C_{BC}(S2) - C_{BC}(S1)\big){V_{in}}^2 \tag{19}$$

If a time series of length ts is observed, an estimation of the power harvested P by the whole system during the observation time ts can be done by counting the number of commutations from S1 to S2, N_{12}, and from S2 to S1, N_{21}, and taking into account the (18)–(19) in the (20) [41]:

$$P = \frac{N_{12}}{ts}E_{AC} + \frac{N_{21}}{ts}E_{BC} \tag{20}$$

The computed values of the parameters of the interdigitated fingers for the mechanical-to-electrical energy conversion are listed in the tab. V. The choice of these values is motivated

by the need to ensure an adequate extraction of energy without affecting the robustness of the fingers and taking into account the movements of the structure between the two stable equilibrium states.

TABLE V
PARAMETERS OF THE ADOPTED MECHANICAL-TO-ELECTRICAL TRANSDUCTION MECHANISM FOR THE DEVICE IN FIG. 20. VALUES ARE EQUAL FOR BOTH THE CAPACITANCES C_{AC} AND C_{BC}.

Variable	Value	Description
N_f	29	Number of fingers on rotor
l_f	150 μm	Total length of each finger
l_{f0}	75 μm	Initial overlap length between two fingers
t	467 μm	Mechanical thickness of each finger
t_f	15 μm	Thickness of the conductive layer
w_f	5 μm	Width of each finger
g	15 μm	Air gap between two fingers

A possible solution to increase the energy harvested in each cycle of commutation E_{AC} and E_{BC} in the (18)–(19) is to increase the difference in the maximum and minimum values of the capacitances C_{AC} and C_{BC}. This can be achieved by exploiting also the thickness of the silicon substrate in the interdigitated capacitors through an adaptation of the BESOI technology process (see fig. 4). The modification consists in the creation of an electrical connection between the single crystal silicon layer and the silicon substrate through a pattern of the buried oxide and a selective deposition of metal (probably aluminium). The creation of suitable trenches in the silicon substrate, from the bottom, and in the single crystal silicon, from the top, ensures the separation of the areas at different electric potential, with also the help of the buried oxide layer. This concept is illustrated in fig. 21.

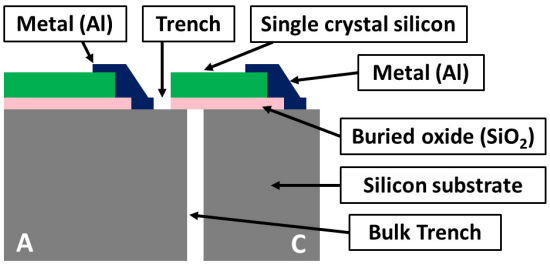

Fig. 21. Basic conceptual schematic of the proposed modifications in the BESOI technology. "A" and "C" represent areas at different electric potential. The picture is not in scale.

Thanks to this modification in the technology process, the thickness of the conductive layer on each finger t_f comes from 15 μm to 465 μm (see fig. 4). This increases the values of the two capacitances C_{AC} and C_{BC} from (13)–(14), the difference between their maximum and minimum values and, from (18)–(19), the amount of the electrical harvested energy.

In order to estimate the power harvested by the whole system from (20) as a benchmark of the proposed concept, the same micro-structures studied in section IV (the bi-stable micro-structure and its "equivalent" mono-stable one) with the same mechanical-to-electrical transducers have been compared in simulations for several accelerations having different associated energy, random dynamics and a spectrum wide about 500 Hz [8]. This range of low frequency vibrations is the most critical to be explored in order to exploit the benefits of the proposed bi-stable device with respect to linear or mono-stable systems. Models in (15)–(20) have been taken into account and parasitic effects are neglected.

As the displacements of the central mass in the mono-stable structure do not always have the same amplitude (neglecting any overshoots) when the device is forced by noisy vibrations, there are no fixed maximum and minimum values for the capacitances C_{AC} and C_{BC} in the system dynamics, differently from the bi-stable device. In order to adopt the models in (15)–(20) and the same strategies of the bi-stable device in the polarization of the capacitances C_{AC} and C_{BC}, two values of displacements t_l to t_h have been imposed as thresholds to control the polarization and the depolarization of the transduction capacitors (in the same way of the positions S1 and S2 in bi-stable device). So, in the mono-stable case, C_{AC} is polarized by V_{in} when the central mass comes from the higher threshold t_h to the lower threshold t_l, analogously C_{BC} is polarized when the system goes from t_l to t_h. Three different pairs of thresholds have been analyzed in the comparisons with the bi-stable device: $t_h = 5\ \mu m$ and $t_l = -5\ \mu m$, $t_h = 10\ \mu m$ and $t_l = -10\ \mu m$ and, finally, $t_h = 13.35\ \mu m$ and $t_l = -13.35\ \mu m$. The last pair ($t_h = 13.35\ \mu m$ - $t_l = -13.35\ \mu m$) presents the same length of displacements between the two equilibrium stable states of the bi-stable device.

Results are presented as the mean values over 30 time series of 100 s each of the power harvested evaluated through (20) for different RMS input accelerations. Fig 22 summarizes the results for $V_{in} = 30\ V$.

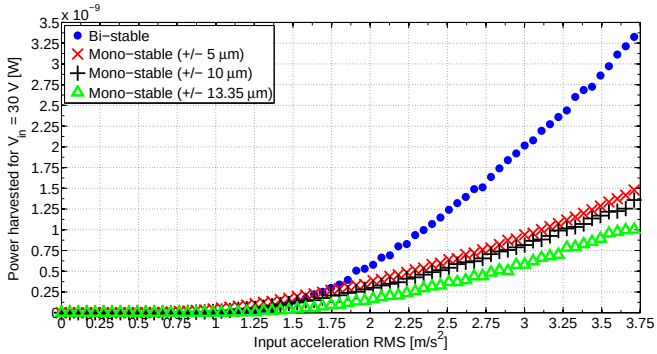

Fig. 22. Power harvested at several RMS value of input acceleration for the bi-stable device and its "equivalent" mono-stable one. A polarization voltage of 30 V and the parameters for the transduction mechanism in the tab. V, with $t_f = 465\ \mu m$, are considered.

Results in fig. 22 confirm the improvement in performance of the bi-stable device over the mono-stable one as soon as the input acceleration is able to put it in commutation between its two stable equilibrium states.

VI. CONCLUSIONS

In this work, an analytical and numerical study of mechanically bi-stable MEMS devices has been proposed in order to harvest kinetic energy more efficiently than traditional linear

resonant or mono-stable micro-generators. Weak, wideband vibrations at low frequencies have been considered. Linear devices are designed to collect kinetic energy at their resonant frequency, therefore arrayed solutions have to be considered to cover large bandwidths. In the case of bistable systems, in order to produce switching between stable states it is sufficient to have an incoming signal whose amplitude allows to pass the "threshold": the frequency is not anymore a fundamental issue. Therefore kinetic energy is collected in a larger frequency range.

Development of these micro-structures has been described together with the process for optimally "shaping" their bi-stable elastic potential.

A complete design is proposed by taking into account a dedicated microfabrication process. Electrostatic energy conversion strategy has been considered from producing electrical output.

In order to have consistent benchmark, the same structure has been considered where design parameters have been chosen such to achieve a monostable behaviour.

In the paper it has been shown as, in the case of bistable device, a larger fraction of mechanical energy is scavenged from input vibrations and transferred to the mechanical-to-electrical transducer.

REFERENCES

[1] S. Priya and D. Inman, *Energy Harvesting Technologies*. Springer Publishing Company, 2008.

[2] R. Torah, P. Glynne-Jones, M. Tudor, T. O'Donnell, S. Roy, and S. Beeby, "Self-powered autonomous wireless sensor node using vibration energy harvesting," *Measurement Science and Technology*, vol. 19, p. 125202, 2008.

[3] V. Raghunathan, A. Kansal, J. Hsu, J. Friedman, and M. Srivastava, "Design considerations for solar energy harvesting wireless embedded systems," in *Proceedings of the 4th international symposium on Information processing in sensor networks*. IEEE Press, 2005, p. 64.

[4] H. Sodano, D. Inman, and G. Park, "Comparison of piezoelectric energy harvesting devices for recharging batteries," *Journal of Intelligent Material Systems and Structures*, vol. 16, no. 10, p. 799, 2005.

[5] S. Anton and D. Inman, "Vibration energy harvesting for unmanned aerial vehicles," in *Society of Photo-Optical Instrumentation Engineers (SPIE) Conference Series*, vol. 6928, 2008, p. 60.

[6] A. Kuo, "Biophysics: Harvesting energy by improving the economy of human walking," *Science*, vol. 309, no. 5741, p. 1686, 2005.

[7] M. Lallart, D. Guyomar, Y. Jayet, L. Petit, E. Lefeuvre, T. Monnier, P. Guy, and C. Richard, "Synchronized switch harvesting applied to self-powered smart systems: Piezoactive microgenerators for autonomous wireless receivers," *Sensors and Actuators A: Physical*, vol. 147, no. 1, pp. 263–272, 2008.

[8] S. Roundy, P. Wright, and J. Rabaey, "A study of low level vibrations as a power source for wireless sensor nodes," *Computer Communications*, vol. 26, no. 11, pp. 1131–1144, 2003.

[9] E. Yeatman, "Energy harvesting from motion using rotating and gyroscopic proof masses," *Proceedings of the Institution of Mechanical Engineers, Part C: Journal of Mechanical Engineering Science*, vol. 222, no. 1, pp. 27–36, 2008.

[10] S. Roundy, "On the effectiveness of vibration-based energy harvesting," *Journal of intelligent material systems and structures*, vol. 16, no. 10, p. 809, 2005.

[11] S. Beeby, M. Tudor, E. Koukharenko, N. White, T. O'Donnell, C. Saha, S. Kulkarni, and S. Roy, "Micromachined silicon generator for harvesting power from vibrations," in *The 4th International Workshop on Micro and Nanotechnology for Power Generation and Energy Conversion Applications (PowerMEMS 2004)*, November 2004, pp. 104–107.

[12] B. Yen and J. Lang, "A variable-capacitance vibration-to-electric energy harvester," *IEEE Transactions on Circuits and Systems I: Regular Papers*, vol. 53, no. 2, 2006.

[13] S. Anton and H. Sodano, "A review of power harvesting using piezoelectric materials (2003-2006)," *Smart Materials and Structures*, vol. 16, no. 3, p. 1, 2007.

[14] S. Beeby, M. Tudor, and N. White, "Energy harvesting vibration sources for microsystems applications," *Measurement science and technology*, vol. 17, no. 12, p. 175, 2006.

[15] T. Sterken, K. Baert, C. Van Hoof, R. Puers, G. Borghs, P. Fiorini, I. MCP, and B. Leuven, "Comparative modelling for vibration scavengers [MEMS energy scavengers]," *Proceedings of IEEE Sensors, 2004.*, pp. 1249–1252, 2004.

[16] P. Mitcheson, E. Reilly, T. Toh, P. Wright, and E. Yeatman, "Performance limits of the three MEMS inertial energy generator transduction types," *Journal of Micromechanics and Microengineering*, vol. 17, p. S211, 2007.

[17] B. Mann and N. Sims, "Energy harvesting from the nonlinear oscillations of magnetic levitation," *Journal of Sound and Vibration*, vol. 319, no. 1-2, pp. 515–530, 2009.

[18] D. Zhu, M. Tudor, and S. Beeby, "Strategies for increasing the operating frequency range of vibration energy harvesters: a review," *Measurement Science and Technology*, vol. 21, p. 022001, 2010.

[19] S. Shahruz, "Design of mechanical band-pass filters for energy scavenging," *Journal of Sound and Vibration*, vol. 292, no. 3-5, pp. 987–998, 2006.

[20] M. Soliman, E. Abdel-Rahman, E. El-Saadany, and R. Mansour, "A wideband vibration-based energy harvester," *Journal of Micromechanics and Microengineering*, vol. 18, p. 115021, 2008.

[21] R. Ramlan, M. Brennan, B. Mace, and I. Kovacic, "Potential benefits of a non-linear stiffness in an energy harvesting device," *Nonlinear Dynamics*, vol. 59, no. 4, pp. 545–558, 2010.

[22] F. Cottone, H. Vocca, and L. Gammaitoni, "Nonlinear energy harvesting," *Physical Review Letters*, vol. 102, no. 8, p. 80601, 2009.

[23] T. Wellens, V. Shatokhin, and A. Buchleitner, "Stochastic resonance," *Reports on Progress in Physics*, vol. 67, no. 1, pp. 45–105, 2004.

[24] M. Ferrari, V. Ferrari, M. Guizzetti, B. Andò, S. Baglio, and C. Trigona, "Improved Energy Harvesting from Wideband Vibrations by Nonlinear Piezoelectric Converters," *Procedia Chemistry*, vol. 1, no. 1, pp. 1203–1206, 2009.

[25] K. Dogheche, B. Cavallier, P. Delobelle, L. Hirsinger, E. Cattan, D. Remiens, M. Marzencki, B. Charlot, S. Basrour, and S. Ballandras, "A bi-stable micro-machined piezoelectric transducer for mechanical to electrical energy transformation," *Integrated ferroelectrics*, vol. 80, no. 1, pp. 305–315, 2006.

[26] B. Andò, S. Baglio, C. Trigona, N. Dumas, L. Latorre, and P. Nouet, "Nonlinear mechanism in MEMS devices for energy harvesting applications," *Journal of Micromechanics and Microengineering*, vol. 20, p. 125020, 2010.

[27] B. Marinkovic and H. Koser, "Smart sand. a wide bandwidth vibration energy harvesting platform," *Applied Physics Letters*, vol. 94, p. 103505, 2009.

[28] D. Nguyen, E. Halvorsen, G. Jensen, and A. Vogl, "Fabrication and characterization of a wideband mems energy harvester utilizing nonlinear springs," *Journal of Micromechanics and Microengineering*, vol. 20, p. 125009, 2010.

[29] S. Jung and K. Yun, "A wideband energy harvesting device using snap-through buckling for mechanical frequency-up conversion," in *Micro Electro Mechanical Systems (MEMS), IEEE 23rd International Conference on*. IEEE, 2010, pp. 1207–1210.

[30] A. Hajati, S. Bathurst, H. Lee, and S. Kim, "Design and fabrication of a nonlinear resonator for ultra wide-bandwidth energy harvesting applications," in *Micro Electro Mechanical Systems (MEMS), IEEE 24th International Conference on*. IEEE, 2011, pp. 1301–1304.

[31] M. Parkinson, B. Jensen, and G. Roach, "Optimization-based design of a fully-compliant bistable micromechanism," *Proceedings of the 2000 ASME Design Engineering Technical Conferences, DETC2000/MECH-14119*, 2000.

[32] P. Boyle, D. Moore, R. Breen, R. Syms, H. Zou, and J. Stagg, "MEMS bistable clamp with electrical locking and release," in *15 th Micromechanics Workshop, MME*, vol. 4, 2005, pp. 5–7.

[33] J. Tsay, H. Chang, and C. Sung, "Design and experiments of fully compliant bistable micromechanisms," *Mechanism and machine theory*, vol. 40, no. 1, pp. 17–31, 2005.

[34] J. Casals-Terre and A. Shkel, "Dynamic analysis of a snap-action micromechanism," in *IEEE Sensors*, 2004, pp. 1245–1248.

[35] L. Howell, *Compliant mechanisms*. Wiley-Interscience, 2001.

[36] B. Andò, S. Baglio, M. Baku, V. Ferrari, E. Sardini, N. Savalli, M. Serpelloni, and C. Trigona, "Numerical and Experimental Investigation

on Contactless Resonant Sensors," *Sensors and Actuators A: Physical*, 2010.
[37] B. Andò, S. Baglio, G. L'Episcopo, V. Marletta, N. Savalli, and C. Trigona, "A be-soi mems for inertial measurement in geophysical applications," *Instrumentation and Measurement, IEEE Transactions on*, no. 99, pp. 1–8, 2011.
[38] V. Lindroos, M. Tilli, A. Lehto, and T. Motooka, *Handbook of Silicon Based MEMS Materials and Technologies*. William Andrew Pub, 2010.
[39] P. Kloeden and E. Platen, *Numerical solution of stochastic differential equations*. Springer, 1995.
[40] R. Lensink, H. Bo, and E. Sterken, *Investment, capital market imperfections, and uncertainty: theory and empirical results*. Edward Elgar Pub, 2001.
[41] S. Meninger, J. Mur-Miranda, R. Amirtharajah, A. Chandrakasan, and J. Lang, "Vibration-to-electric energy conversion," *Very Large Scale Integration (VLSI) Systems, IEEE Transactions on*, vol. 9, no. 1, pp. 64–76, 2001.
[42] S. Baglio, S. Castorina, and N. Savalli, *Scaling issues and design of MEMS*. Wiley Online Library, 2007.
[43] Y. Cho, A. Pisano, and R. Howe, "Viscous damping model for laterally oscillating microstructures," *Microelectromechanical Systems, Journal of*, vol. 3, no. 2, pp. 81–87, 1994.
[44] P. Mitcheson, T. Sterken, C. He, M. Kiziroglou, E. Yeatman, and R. Puers, "Electrostatic microgenerators," *Measurement & control*, vol. 41, no. 4, p. 114, 2008.

Bruno Andò received the M.S. degree in electronic engineering and the Ph.D. degree in electrical engineering from the Universit di Catania, Catania, Italy, in 1994 and 1999, respectively. From 1999 to 2001, he was a Researcher with the Electrical and Electronic Measurement Group, DIEES, now the DIEEI, University of Catania, where he has been an Assistant Professor since 2002. He holds several national and international scientific collaborations. He teaches courses in Measurement Theory, Electronic Instrumentations and Sensors and Transducers. During his activity, he has coauthored more than 200 scientific papers, presented in international conferences and published in international journals and books. His main research interests are sensor design and optimization, microelectromechanical system and nanosystem, multisensors architecture for Ambient Assisted Living, new materials for sensors, nonlinear techniques for signal processing with particular interest in stochastic resonance and dithering applications, and distributed measurement systems for environmental monitoring.

Salvatore Baglio received the M.S. degree and Ph.D. degree from the University of Catania, Catania, Italy, in 1990 and 1994, respectively. He was a Lecturer of Automatic Control Theory with the University of Messina, Messina, Italy, and of Electronic Measurement Systems with the University of Catania. Since 1996, he has been with the DIEES, now the DIEEI, University of Catania, where he is currently an Associate Professor of Electronic Instrumentations and Measurements. He is a coauthor of several scientific publications, including papers that were published in international journals or presented at international conferences, and chapters in books. He is also the holder of several U.S. patents. His research interests are mainly focused on measurement methodologies, smart sensors, microsensors, and microsystems.

Gaetano L'Episcopo was born in Catania, Italy, in 1983. He received the B.S. degree in Electronics Engineering and the M.S. degree in Automation Engineering and Control of Complex Systems in 2006 and 2010, respectively, from the University of Catania, Catania, Italy. He is currently working toward the Ph.D. degree in the DIEEI at the University of Catania, Catania, Italy. His research interests include microelectromechanical-system devices for sensors and actuators, nonlinear devices for energy harvesting and nanotechnology.

Carlo Trigona received the M.S. degree in Automation Engineering and Control of Complex Systems and the Ph.D. degree in Electronic, Automation and Control of Complex System from University of Catania, Catania, Italy in 2006 and 2009 respectively. He spent a post-doc period at LIRMM University Montpellier II, France where he worked on RF-MEMS and energy harvesters (2010-2011). He is currently a research associate at DIEEI, University of Catania. He is co-author of more than 60 scientific publications, which include chapters in books, papers in international journals and proceedings of international conferences. His research interests include microsystems and microsensors, fluxgate magnetometers and energy harvesting.